Traceable interferometry using binary reconfigurable holograms

M. T. Cashmore,[1,*] S. R. G. Hall,[1] and G. D. Love[2]

[1]National Physical Laboratory, Hampton Road, Teddington, Middlesex, UK

[2]Centre for Advanced Instrumentation, Durham University Physics Department, South Road, Durham, UK

*Corresponding author: matt.cashmore@npl.co.uk

We describe the characterization of a ferroelectric-liquid-crystal-on-silicon (FLCOS) spatial light modulator (SLM) in the production of holograms for use in interferometric metrology. It has already been shown that such a device can be used in producing small-amplitude arbitrary reference surfaces with small but appreciable errors due to the contaminating effect of higher-order structures being propagated through the spatial filter. Here we further quantify the size of these residuals for increasingly large aberrations up to nine waves rms Zernike astigmatism, showing a Zernike-corrected rms wavefront error of roughly 0.06 waves with high vibrational stability. We also present measurements of a vacuum window element using the FLCOS device to drastically reduce interferometric fringe density, showing a residual wavefront error of 0.046 waves rms with dominant components originating from test piece structure rather than holographic errors.

OCIS codes: (090.0090) Holography; (090.1760) Computer holography; (090.2880) Holographic interferometry; (110.3175) Interferometric imaging; (120.3940) Metrology.

http://dx.doi.org/10.1364/AO.53.005353

1. Introduction

Interferometry is a long-established and widely used technique in optical surface metrology; however, it is commonly found that the surface under test deviates significantly from the form of any highly accurate, readily available reference surface. In particular, highly curved freeform surfaces can deviate from a reference shape sufficiently as to render the detection of well-sampled fringes highly problematic. This requires that a means of compensating for this freeform surface be incorporated in the interferometer.

Computer-generated holograms (CGHs) have been successfully used as nulling elements in interferometry for many years [1–3] and are a valuable tool in expanding the dynamic range of the technique. One drawback to the standard method of production using e-beam lithography or thermochemical writing processes is that the design is necessarily optimized for testing of a single optical surface.

Ferroelectric-liquid-crystal-on-silicon (FLCOS) spatial light modulators (SLMs) allow for the implementation of rapidly reconfigurable holograms into an interferometric system [4], which enables the optical wavefront in one arm of the interferometer to be arbitrarily distorted on demand to compensate for a variety of optical surfaces. These devices can also add new flexibility to the incorporation of well-known phase shifting techniques [5], as the phase steps can be programmed directly into the holographic display, and thus eliminate the need for separate phase-shifting elements. The binary nature of the FLCOS SLM also negates the need for a fully profiled understanding of the pixel response function as required by nematic-phase-only liquid crystals, as any deviation from the ideal relative phase modulation of 0 and π reduces the efficiency of the device rather than increasing holographic form error. FLCOS devices have been shown to be capable of producing low-amplitude aberrations such as 2 rad defocus with an accuracy of 0.045 waves rms [6], and this paper builds upon this to examine their behavior when producing much larger quantities of aberration.

2. Theory and Simulation

A circular hologram of radius 500 pixels (where one pixel = 13.65 mm) is displayed on the SLM, containing the desired wavefront aberration $\phi_D(x,y)$ along with 45 waves Zernike tip and tilt, $\tau(x,y)$, used to spatially separate the diffracted orders in the Fourier plane. Tilts larger than 45 waves were avoided, as above this value the corresponding binarized grating thickness was observed to decrease to below the minimum required for Nyquist sampling, and using equal values for X and Y tilt allowed for maximal separation of orders in the Fourier plane. The desired phase profile, ϕ_D, is transformed into a binary representation, which is displayed on the SLM according to [4]

$$\phi_B(x,y) = \begin{cases} \pi & \text{if } \cos \phi(x,y) \geq 0 \\ 0 & \text{otherwise} \end{cases}, \quad (1)$$

where $\phi_B(x,y)$ is the pattern to be displayed and $\phi(x,y) = \phi_D(x,y) + \tau(x,y)$.

The complex amplitude of a wavefront containing this profile now holds the property of a square wave. The Fourier transform of square waves can be represented as an infinite sum of odd exponential functions [4,7]:

$$F[\phi_B] \approx \exp[i(\phi_D + \tau)] + \exp[-i(\phi_D + \tau)]$$
$$- \frac{1}{3}\exp[3i(\phi_D + \tau)] - \frac{1}{3}\exp[-3i(\phi_D + \tau)]\dots\dots$$
$$(2)$$

We note here that the exponent of each term contains the analog phase distribution ϕ_D of our desired wavefront. We can physically reproduce this expansion by passing the binarized wavefront through a lens, and using a spatial filter in the focal plane, we isolate the first-order spot and reimage to obtain a wave with an analog phase profile ϕ_D. We therefore can create a wavefront with a continuous phase profile by spatially filtering a square-wave profile.

The transmission matrix of a digital SLM is necessarily discontinuous due to the binary pixelated nature of its phase modulation. A discontinuous phase profile, as shown in Eqs. (1) and (3), contains high-order modes generated by the square-wave form of the complex amplitude. The design of the transmission matrix is driven by the requirement to remove these higher-order modes, leaving only lower orders producing the desired continuous phase profile.

It is important to use a sufficiently large spatial filter, as seen in Fig. 2, to enable the entire point spread function (PSF) of the desired order to pass, while still excluding higher-order diffracted terms in the reconstructed wavefront. If we allow through higher-order harmonics, we see well-defined artifacts in the recovered phase maps which comprise a significant portion of the residual wavefront error. It has been suggested this can be mitigated through the use of an alternate binarization technique, to break up the highly structured diffraction pattern

through the inclusion of random background noise as [6]

$$\phi_B(x,y) = \begin{cases} \pi & \text{if } \cos \phi(x,y) \geq \text{rand}(-1:1) \\ 0 & \text{otherwise} \end{cases}. \quad (3)$$

It is also possible to reduce the effect of higher-order contamination through the use of three-step phase-shifting interferometry; as each phase step is $2\pi/3$, all orders which are multiples of 3 are eliminated entirely from the reconstructed phase map.

A simulation of an interferometer using the FLCOS device to display binary holograms was written to evaluate the accuracy to which increasingly aberrated wavefronts could be produced via this method. We use discrete Fourier transforms on the oversampled binary wavefront and apply a spatial filter of size 4.1 mm to ensure we fully transmit the desired aberration. The optical set up used in this fashion is in a 2f arrangement, with the hologram at the front focal plane of the transform lens, and the spatial filter placed at the back to ensure a 1-to-1 scaling relation between the object and image size. This also allows us to quantify the effect of allowing unchecked higher-order harmonics to pass through the filter and create artifacts in the recovered phase distribution. We can see from [8] that this size aperture is sufficient to reproduce up to nine waves Zernike astigmatism and trefoil to within $\lambda/50$ residual rms error. Smaller pinholes are more suited to lower-magnitude aberrations. This larger pinhole size is then used experimentally to conservatively allow for measurement uncertainty arising from aperture adjustment. Maintaining the same aperture size improves the repeatability of measurement for the range of holograms produced. Inverse Fourier transforms are used to recover the wavefront from the filtered Fourier plane and then calculate the fringe pattern expected using a reference wavefront corresponding to a flat surface. The desired aberration is removed after the implementation of three-step interferometry techniques to the simulated fringe pattern, to quantify the errors produced alongside the intended phase distribution. Figure 1 shows the growth of residual wavefront rms for a null interferogram of increasingly large quantities of astigmatism and trefoil being encoded onto the hologram, using the standard binarization technique in Eq. (1). The initial rise in the rms error is ascribed to a combination of contaminating higher orders being passed through the pinhole, the spatial quantization error due to the finite resolution of the SLM, and the energy leaking from orders within the spatial filter. In this paper, no attempt has been made to decouple or quantify the contributions of these error sources separately. For every aberration displayed on the hologram, there is a corresponding optimum-sized spatial filter value which is just sufficient to pass the desired diffracted order while allowing through a minimum of higher harmonics. Above this optimum size, the relative contribution of aliased orders
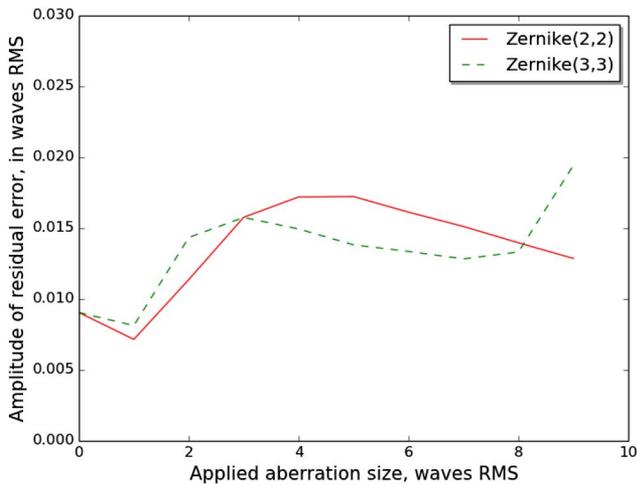
Fig. 1. Simulated interferometric residual wavefront errors after the removal of applied aberration for increasing quantities of astigmatism and trefoil on an applied hologram with a constant spatial filter size of 4.1 mm.

compared to the desired first order increases. We believe the decrease in residual rms seen in Fig. 1 is due to the fixed spatial filter size used being more appropriate for the passage of the larger astigmatic aberrations, as it is closer to the optimum filter size for those holograms. This error then sharply rises once more, as seen for the behavior of the trefoil propagation, when the filter is insufficiently sized to pass the full PSF of the desired wavefront. If we optimize the spatial filter size for an aberration of five waves rms Zernike astigmatism, we see a residual rms error of 0.01 waves in the reconstructed wavefront for a spatial filter size of 1.6 mm.

3. Experimental Results

Experimental characterization of the FLCOS device was performed using the same-sized hologram as above, in a Mach–Zehnder interferometer using a 632.8 nm He–Ne laser for illumination, as shown in Fig. 2. Of note is that our spatial filter is located
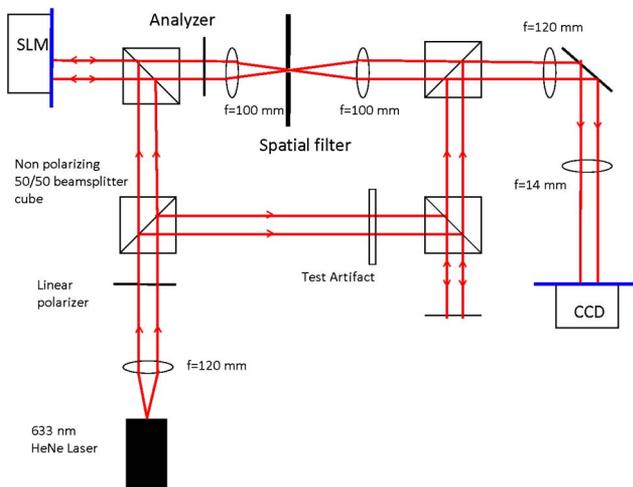
Fig. 2. Experimental Mach–Zehnder setup used in the characterization of the binary FLCOS SLM.

in the focal plane of the first lens, and both the hologram and the CCD are located in planes conjugate to each other. A mirror is located in the arm the SLM is not in, in order to allow for path length matching between the two arms. Three-step interferometry was implemented using the SLM to display three phase-shifted holograms in sequence, and with waveform signal generators to synchronize hologram production with camera integration times. We make use of the fast switching speeds available using the FLCOS SLM to record 200 μs exposure fringe patterns to reduce the impact of vibration on the accuracy of the reconstructed wavefront. For increasingly astigmatic holograms, we observe accurate recovered aberration growth, as can be seen from Table 1, along with nulled residual wavefront errors which increase as a function of applied aberration size. We also observe a robust insensitivity to vibrational effects through repeat measurements, showing a mean deviation of 3×10^{-4} waves in residual rms error.

While Table 1 shows the presence of significant errors in the nulled phase map, we observe that through the removal of the first 20 Zernike terms, we obtain a roughly constant residual error of 0.06 waves rms. It can also be seen from Fig. 3 that the presence of higher-order structure from the passing of unwanted terms through the spatial filter is evident in the recovered null phase map. We also measure the growth of the residual wavefront rms for the same series of astigmatic holograms using the random binarization technique seen in Eq. (3), to encode the hologram onto the SLM and observe that this successfully eliminates the presence of contaminating structure even though this is at the cost of increased residual error. We can see this for the case of five waves astigmatism in Fig. 4, and can also clearly see that there are significant artifacts in the unwrapped phase map for the random binarization technique which are induced by the local phase unwrapping approach [8]. We also compare the residual errors obtained through recovering the phase map using both a local and global [9] phase unwrapping technique and compare their relative merits.

Figure 5 shows the growth of residual error for two different binarization techniques with two distinct phase unwrapping approaches. The local unwrapping approach along with the standard binarization algorithm gives us the most accurate production of Zernike astigmatism; however, for the random binarization this local approach incurs large errors. These may be due to the introduction of features in the wrapped phase pattern which the unwrapping algorithm cannot process; these occur as a direct result of increasing the random noise in the hologram. Small errors are then propagated into large islands of erroneous phase value due to the localized nature of the algorithm. It is therefore necessary to compare the two binarization methods using a phase unwrapping algorithm that can successfully process both. Doing so using a global method unwraps both without the addition of large error terms or artifacts. This

Table 1. Production of Zernike Astigmatism Using a Standard Binarization Technique

Applied Aberration Size (Waves rms)	1	2	3	4	5	6	7	8	9
Measured astigmatism	0.9994	1.9976	2.9946	3.9923	4.9913	5.9912	6.9927	7.9940	8.9964
Residual error [a]	0.1170	0.1209	0.1391	0.1582	0.1680	0.1931	0.2301	0.2497	0.2855

[a]Residual error is the error after subtraction of the ideal applied aberration size, and repeated measurements show an average standard deviation of 3×10^{-4} waves rms deviation.

allows us to see that the inclusion of randomized background noise gives us a larger residual error than allowing for the effect of higher-order structure propagating through the system. Compensation for the production of unwanted Zernike terms via the subtraction of a modal deconstruction of the recovered phase map reveals that the residual rms error is roughly constant for increasing magnitudes of applied aberration, provided that the spatial filter is transmitting the full extent of the first-order diffracted term. This subtraction of the calculated Zernike modes in the resultant phase map allows the isolation of the errors in the phase profile encoded in the hologram from the effects of higher-order aliasing and intensity modulation contamination.

There is a significant increase in the residual rms error from the experimental results in Fig. 5 as compared to the simulation in Fig. 1. The major source of this discrepancy is that the simulation does not take into account camera noise, which adds approximately 0.02 waves rms Poissonian noise into the simulated results. Furthermore, the experimental phase maps show a degree of intensity modulation, which will not be observed in the simulation. The roughly flat behavior of the residual error for the case of the standard, locally unwrapped binarization technique, in contrast to the shape of the simulated residuals, implies that higher-order aliasing in the

recovered maps is not dominating our error. If it were, we would expect to see the behavior of our residual errors match that seen in Fig. 1.

Further evaluation of the use of a FLCOS SLM to be used as a nulling optic in the interferometric measurement of surface forms was carried out by measuring the phase map of a wavefront passing through a vacuum window, using subaperture stitching to obtain a composite phase map of an area larger than the beam width. Attempts to characterize the phase aberrations introduced by the vacuum window using a standard Zygo interferometer proved unsuccessful due to a combination of poor fringe modulation and high fringe density in the recorded interferograms. A hologram of 8 waves of X tilt and 1 wave of Y tilt as well as first wave Zernike defocus, was displayed on the SLM to null out a significant proportion of the fringe pattern. This was done in order to obtain well-sampled measurements of each subaperture before stitching them into a full map of the area of interest. We measure the wavefront produced from spatially filtering the desired diffraction spot to identify the erroneously produced Zernike terms, which are used to correct the desired phase map and remove hologram production errors from final measurements.

Figure 6 shows the residual phase map after Zernike correction for the composite vacuum window measurement, which reveals low-amplitude structure inherent in the optic independent from errors in the hologram. Through the use of a nulling hologram, we observe a 10% reduction in the magnitude of the residual rms wavefront error, down to 0.046 waves. We see that the dominant source of this residual is from the structure seen on the optic rather than from phase discontinuities introduced through the stitching process, which are reduced through averaging over multiple subapertures and Fourier-filtering the phase map to reduce high-frequency variations from camera noise. We argue that the structural features seen, which resemble ringing, are directly due to the window rather than the hologram, as they are seen to be continuous between overlapping subapertures, and the window is the only element translated between measurements. By reducing the fringe density using a static hologram throughout the measurement, any nonstandard artifacts would not be continuous between neighboring subapertures, but instead repeated. By removing standard Zernike polynomials from the recovered phase map, we can show that the use of the FLCOS device to produce nulling holograms which reduce fringe density is not the limitation in the measurement of low-amplitude, nonstandard form

6.8mm

0.6–0.4 –0.2   0   0.2   0.4   0.6
Amplitude in waves
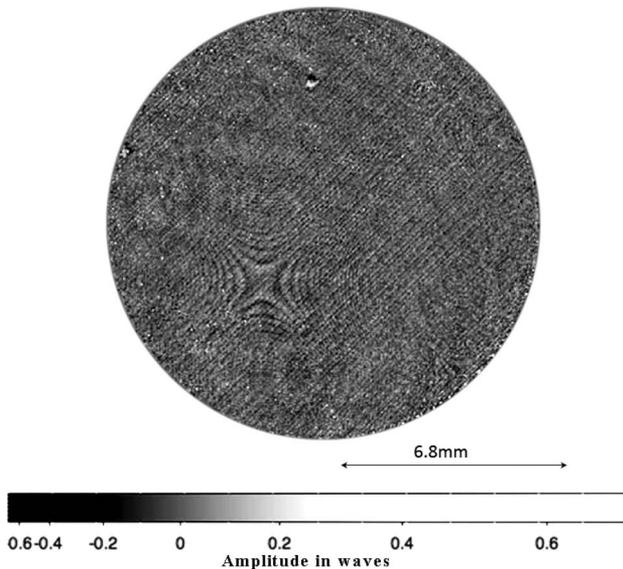
Fig. 3. Recovered experimental nulled phase map for a hologram of five waves Zernike astigmatism, without any test artifacts, showing the presence of higher-order astigmatic structure. The amplitude scale is in waves, with some nonlinearity introduced to improve visibility.
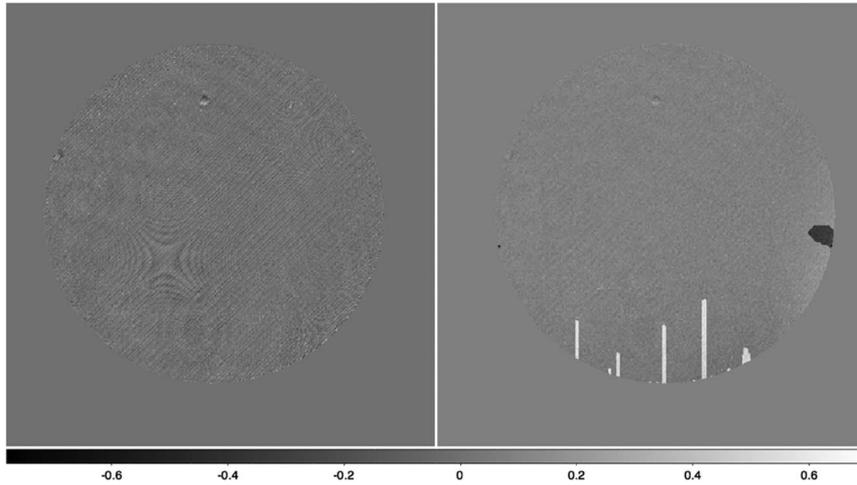
Fig. 4. Comparison of the unwrapped phase profile for five waves astigmatism post-Zernike correction between the standard (left) and random (right) binarization techniques, with the Z scale given in waves. We can see in this that despite the elimination of higher-order aliasing effects, the random binarization incurs severe errors in the phase unwrapping procedure.

deviations. Through simulating the propagation of the desired wavefront and allowing for camera noise, we expect a limiting residual rms of 0.036 waves for the current experimental configuration, which is not significantly less than the residuals observed.

In order to add a degree of traceability to the interferometric use of the FLCOS device, a comparison between the measurements of a high-quality transmissive window and a $f = 2500$ mm focal length lens taken on a Zygo interferometer was made. After the removal of tip and tilt terms, the rms wavefront error measured on the Zygo was found to be 0.043 waves rms, compared to the SLM interferometer result of 0.048 waves. A fully Zernike compensated rms measurement of the two results shows a relative residual error of 0.007 and 0.045 waves rms.

Measurement of the phase map of the test lens, however, was complicated due to the difficulty in obtaining a suitable reference surface for the Zygo

interferometer. Testing weak lenses in this manner requires an extremely long bench, as well as a large-radius-of-curvature reference mirror to reflect the beam back to the Zygo camera. As a result of this, a phase map was not produced for the weak lens; however, a focal length measurement was made with a value of 2563.651 mm and uncertainty of ± 0.264 mm, with a coverage factor of $k = 2$ to allow calculation of the expanded uncertainty. This value of k will give a level of confidence of approximately 95% assuming a normal distribution [10]. Using the SLM interferometer, a phase map of the lens was produced, as it is uniquely suited to the task of nulling the focusing power of very weak lenses without any reconfiguration of the optical setup. From a measurement of the Zernike defocus term in the recovered phase map, the focal length was calculated to be 2565 ± 12 mm, which agrees within the uncertainties of the SLM interferometer measurement.
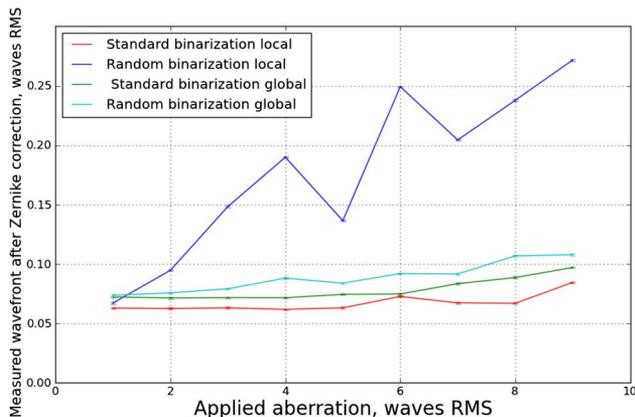
Fig. 5. Experimentally measured Zernike corrected wavefront residuals for increasingly astigmatic holograms, comparing the two proposed binarization techniques via both a global and a local phase unwrapping algorithm. Uncertainty in the results from repeated measurements is seen to be 3×10^{-4}, resulting in error bars which are difficult to resolve in the graph, as they are relatively small.
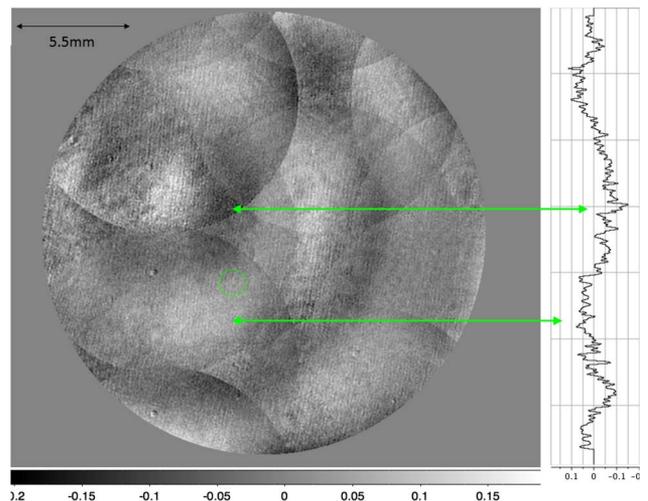
Fig. 6. Composite phase map of residual structure seen in vacuum window measurements after Zernike correction, revealing the presence of low-amplitude large-scale features which dominate the recovered wavefront rms.

4. Conclusion

In conclusion, we have shown the ability of an FLCOS SLM to produce known reference waves with small errors, over a larger range of applied magnitude aberrations than previously investigated. Aliased artifacts are not as detrimental to wavefront accuracy as previously thought, provided sufficient separation of diffracted orders in the Fourier plane is achieved, and therefore the introduction of random background noise and a subsequent increase in the required number of images taken are not necessary. We also show that the use of an FLCOS SLM in interferometric metrology to null fringe density does not incur serious aberration into the measured results, and we have provided a comparison with standard interferometry which allows traceability of the measurements to national standards. This method shows promise for the development of a more versatile instrument than a standard interferometer while being more cost effective than the manufacture of multiple bespoke lithographically produced CGHs.

References

1. A. Ono and J. C. Wyant, "Aspherical mirror testing using a CGH with small errors," Appl. Opt. **24**, 560–563 (1985).
2. J. H. Burge, "Applications of computer-generated holograms for interferometric measurement of large aspheric optics," Proc. SPIE **2576**, 258–269 (1995).
3. J. H. Burge, "Efficient testing of off-axis aspheres with test plates and computer generated holograms," Proc. SPIE **3782**, 348–357 (1999).
4. M. Neil, M. Booth, and T. Wilson, "Dynamic wave-front generation for the characterization and testing of optical systems," Opt. Lett. **23**, 1849–1851 (1998).
5. K. Creath, "Phase measurement interferometry techniques," in *Progress in Optics* (Elsevier, 1998), Vol. **26**, pp. 349–393.
6. B. R. Boruah, G. D. Love, and M. A. A. Neil, "Interferometry using binary holograms without high order diffraction effects," Opt. Lett. **36**, 2357–2359 (2011).
7. W. Lee, "Binary computer-generated holograms," Appl. Opt. **18**, 3661–3669 (1979).
8. M. T. Cashmore, "Interferometric metrology using reprogrammable binary holograms," Ph.D. thesis (Durham University, 2013).
9. M. Schofield and Y. Zhu, "Fast phase unwrapping algorithm for interferometric applications," Opt. Lett. **28**, 1194–1196 (2003).
10. JCGM, 100:2008 "Evaluation of measurement data—guide to the expression of uncertainty in measurement," (2008).